Study of Benzylperoxy Radical Using Laser Photolysis: Ultraviolet Spectrum, Self-Reaction, and Reaction with HO_2 Kinetics

G. El Dib,* A. Chakir, E. Roth, J. Brion, and D. Daumont

Laboratoire GSMA, UMR CNRS 6089, Faculté des Sciences, Université de Reims, Moulin de la Housse, B.P. 1039, 51687 REIMS Cedex 2, France

Received: November 25, 2005; In Final Form: April 5, 2006

The ultraviolet absorption spectrum of benzylperoxy radical and the kinetics of the reactions $2C_6H_5CH_2O_2 \rightarrow$ products (I) and $C_6H_5CH_2O_2 + HO_2 \rightarrow$ products (II) are studied. Experiments are carried out using the laser photolysis technique with time-resolved UV−visible absorption spectroscopy over the temperature range 298−353 K and the pressure range 50−200 Torr. The UV spectrum is determined relative to the known cross section of the ethylperoxy radical $C_2H_5O_2$ at 250 nm. Using factor analysis, the spectrum obtained is refined and the concentrations of the main absorbing species are extracted. The kinetic parameters are determined by analyzing and simulating the temporal profiles of the species concentrations and the experimental optical densities in the spectral region 220−280 nm. These are obtained using the recent UV spectra of the absorbing species existing in our mechanism. The Arrhenius expressions for reactions I and II are (cm^3·$molecule^{-1}$·s^{-1}) $k_I = 2.50 \times 10^{-14}e^{1562/T}$ and $k_{II} = 5.70 \times 10^{-14}e^{1649/T}$. Our results are discussed and compared to literature data.

I. Introduction

Aromatic compounds are released into the atmosphere by various sources (e.g. paint solvents, vehicle exhausts, etc.)[1−3] and act as primary pollutants. They represent a large amount of non-methane hydrocarbons (NMHC).[4,5] Moreover, these compounds are effective reagents which significantly contribute to urban pollution. To understand their reactivity and their photooxidation mechanism, it is necessary to know the kinetic and spectroscopic behavior of their derived primary aromatic peroxy radicals.

Extensive progress has been made in the knowledge of peroxy radical kinetics. The results concerning these species were reported in the literature.[6−9] However, little information is available about the reactivity of aromatic peroxy radicals. In the atmospheric oxidation of toluene, one of the most aromatic compounds emitted into the atmosphere,[10] the contribution of benzylperoxy radical, $C_6H_5CH_2O_2$, derived from this oxidation, is not negligible. To date, only one kinetic study is available in the literature concerning this species.[11] To reduce the uncertainty and to enrich data concerning this compound, we have undertaken its study. In this work, we report the UV absorption spectrum of the benzylperoxy radical and the kinetics of the following reactions:

$$2C_6H_5CH_2O_2 \rightarrow \text{products} \quad \text{(I)}$$

$$C_6H_5CH_2O_2 + HO_2 \rightarrow \text{products} \quad \text{(II)}$$

The study of this radical follows previous work concerning the ethylperoxy radical,[12] $CH_3CH_2O_2$, the chloroethylperoxy radical,[13] $ClCH_2CH_2O_2$, and the β-hydroxy peroxy radical,[14] $(CH_3)_2C(OH)CH_2O_2$. Studying the benzylperoxy radical will enable us to determine the effect of the aromatic group on the reactivity of the peroxy radical.

The experimental technique used in this work is laser photolysis with time-resolved absorption UV−visible spectroscopy.

To complete the analysis of our results and to be more accurate, we have used the numerical technique of factor analysis in our calculations. To our knowledge, this work provides the first kinetic study using factor analysis in the exploitation of the experimental data obtained by flash/laser photolysis in the atmospheric field.

II. Experimental Section

A. Experimental Apparatus. The experimental setup of the laser photolysis/UV absorption used in this study is shown in Figure 1. The reactor is a double-jacket Pyrex cell, 56 cm in length and 2.5 cm in diameter, equipped with quartz windows. The temperature regulation is provided by a fluid circulating between the inner wall and the second jacket. The fluid circulation is commanded by a LAUDA Ultras RUK thermostat which permits better control over the heating or cooling power by circulating fluid (water, ethanol). The working temperature range of the thermostat is −50 to +100 °C, the temperature control is ±0.05 °C, and the flow rate was set at a maximum of 15 L/min.

The photolysis pulse is provided by an excimer laser (Lambda-Physik COMPex 201) operating at 351 nm. The laser produces 40 ns pulses with energies from 80 to 300 mJ at a maximum repetition rate of 10 Hz. The photolysis laser beam (rectangular cross section, 2.5 cm × 1 cm) passes longitudinally through the reaction cell. It is steered along and out of the reactor using dichroic reflectors (Melles Griot Ltd).

The light source is a 30 W deuterium lamp providing a continuum extending from 200 to 400 nm. After being focused by means of a lens−mirror system, the light goes through the

* To whom correspondence should be addressed. E-mail: gisele.el-dib@univ-reims.fr.

10.1021/jp056860p CCC: $33.50
Published on Web 06/07/2006

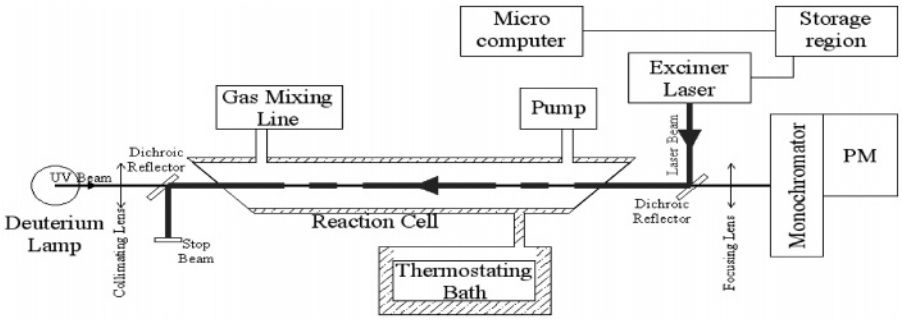

Figure 1. Schematic of the experimental setup.

cell and the emerging beam is analyzed by a Jobin-Yvon monochromator (focal length, 245.76 mm; aperture, F/4.1; blazed grating, 1200 lines/mm; dispersion, 3 nm/mm; resolution, 0.1 nm). The signal is detected by a R928 Hamamatsu photomultiplier tube. After amplification, the signal is captured after each shot by a digital storage oscilloscope (PICO ADC-212), and the data are transferred to a computer for storage. The computer is also used to command the trigger pulse of the laser. The reaction mixture is renewed between consecutive laser shots to avoid the products' accumulation. So, the time between consecutive pulses was set to exceed gas residence time. To improve the signal-to-noise ratio of the data, the signal intensity vs time profiles were averaged over 300 to 1000 laser shots for each wavelength setting of the monochromator under study. The wavelength calibration is achieved by using a low-pressure mercury lamp.

Steady gas flows were maintained by calibrated gas flow controllers. The pressure in the reactor is controlled by a 0−1000 mbar MKS Baratron capacitance manometer. The temperature inside the cell is given by two platinum resistance temperature sensors (Pt 100-DIN 43760) for use between −70 and +200 °C. The sensors were positioned on the extremities of the cell. The temperature gradient did not exceed 0.5 °C.

B. Experimental Conditions. The benzylperoxy radical is generated by photolysis of a slow flowing Cl_2, N_2, O_2, and $C_6H_5CH_3$ mixture via the following reactions:

$$Cl_2 + h\nu \rightarrow 2Cl$$

$$Cl + C_6H_5CH_3 \rightarrow C_6H_5CH_2 + HCl \qquad (IV)$$

$$C_6H_5CH_2 + O_2 + M \rightarrow C_6H_5CH_2O_2 + M \qquad (V)$$

As explained by Nozière et al.,[11] reaction IV proceeds entirely by H-abstraction to form benzyl radical in a 100% yield. To have a fast conversion of the chlorine atoms, to minimize the effect of secondary reactions and to avoid products' accumulation, the initial $C_6H_5CH_3$ concentration must be a few orders of magnitude lower than that of O_2 and at least equal to the initial concentration of Cl_2 ($[O_2] \gg [C_6H_5CH_3] \approx [Cl_2]$).

To study reaction II, methanol was added to generate hydroperoxy radical as follows:

$$Cl + CH_3OH \rightarrow CH_2OH + HCl \qquad (VIII)$$

$$CH_2OH + O_2 \rightarrow CH_2O + HO_2 \qquad (IX)$$

Toluene and methanol were premixed with nitrogen in a 10 L glass bulb to form a 0.5−1.2% mixture at a total pressure of about 1000 Torr. The concentrations of the reagents were calculated from their mass flow rates, the temperature, and the pressure in the reaction cell. All flow rates were measured with mass flow meters calibrated by measuring the rate of pressure increase in a known volume. To verify the constancy of the concentrations of Cl_2 and toluene in the cell during the experiment, the concentrations of these species were determined optically before and after each experiment, by measuring the absorption of Cl_2 at 330 nm ($\sigma_{Cl_2} = 2.56 \times 10^{-19}$ molecule^{-1}·cm^2)[15] and the absorption of toluene at 260 nm ($\sigma_{toluene} = 5.31 \times 10^{-19}$ cm^2·molecule^{-1}, determined in our laboratory). During each experiment the concentration variation did not exceed 10%.

All experiments were performed within the following range of initial conditions: temperature, 298−353 K; pressure, 50−200 Torr; optical path, 56 cm. The reagents concentrations (in molecule·cm^{-3}): $[Cl_2] = (0.3-15) \times 10^{15}$; $[O_2] = (0.3-2) \times 10^{18}$; $[C_6H_5CH_3] = (0.3-8) \times 10^{16}$; $[CH_3OH] = (0.3-8) \times 10^{16}$.

In these conditions, the concentrations of the intermediate absorbing species were between 0.50×10^{14} and 1.00×10^{14} molecule·cm^{-3}.

The reagents used are obtained from the following sources: Cl_2 (1% in N_2 pure), O_2 (99.999% pure), C_2H_6 (99.999% pure) provided by Air Liquide; toluene (99.8%) and methanol (99.8%) provided by Aldrich. All the reagents are used without further purification.

III. Temporal Profile Analysis

In the spectral range 245−280 nm, the absorption of benzylperoxy radical is important relative to the other absorbing species. Therefore, the signal obtained in this region decreases with time. However, the signal profile below 245 nm increases with time, because of the strong absorption of the stable products (such as benzaldehyde) resulting from the photolysis.

Figure 2a,b shows a typical trace of optical density (OD) vs time, following the photolysis of a mixture of Cl_2, N_2, O_2, and $C_6H_5CH_3$ at 220 and 260 nm, respectively. The signal results from the absorption of several species corresponding to a time-dependent total optical density (OD) such that

$$(OD)_{\lambda,total} = \Sigma(OD)_{\lambda,m} = f(t) \qquad (1)$$

where m is the absorbing species (m = $C_6H_5CH_2O_2$ (RO_2), HO_2, H_2O_2, C_6H_5CHO (R′CHO), $C_6H_5CH_2OOH$ (ROOH), $C_6H_5CH_2$-OH (ROH), $CH_3C_6H_5$).

The optical density is related to the concentration C_m according to Beer−Lambert's law:

$$(OD)_{\lambda,m} = \sigma_{\lambda,m} \cdot l \cdot C_m \qquad (2)$$

Here l = absorption path and $\sigma_{\lambda,m}$ = absorption cross section at the wavelength λ for the species m.

In this work, we used two methods to analyze the temporal profiles. The first one, called the "classical method", uses only a part of the experimental signal to extract the RO_2 cross

sections. The second one, called "factor analysis" (FA), treats the whole signal at different wavelengths simultaneously to extract the cross sections, the number, and the concentrations of the main absorbing species.

A. Classical Method. *A.1. Determination of the Benzylperoxy Spectrum.* To determine the cross-section values of the benzylperoxy radical, experiments were carried out under conditions of low HO_2 concentration (no methanol was added). The cross sections of the benzylperoxy radical were obtained relative to the absorption cross section of the $CH_3CH_2O_2$ at 250 nm, which is fairly well-known ($\sigma_{250,C_2H_5O_2}$ (cm^2·$molecule^{-1}$) = 4.12×10^{-18}).[9] We have proceeded as follows:

In each experiment, the toluene was replaced, in the gas mixture, by C_2H_6 using the same experimental conditions (chlorine concentration, laser energy, pressure, etc.) to produce the same initial concentration of peroxy radical. Thus, the ratio of the initial optical densities leads to the calculation of the benzylperoxy cross section according to the relation

$$\sigma_{\lambda,RO_2}/\sigma_{250,C_2H_5O_2} = ([OD]_{\lambda,RO_2})_0/([OD]_{250,C_2H_5O_2})_0 \quad (3)$$

where σ_{λ,RO_2} is the absorption cross section of the benzylperoxy radical at the wavelength λ and $([OD]_{\lambda,RO_2})_0$ and $([OD]_{250,C_2H_5O_2})_0$ are the initial optical densities of benzylperoxy and ethylperoxy radicals, respectively.

It is important to note that the signal obtained is influenced by the consumption of toluene. In fact, the loss of toluene significantly affects the initial OD of RO_2 (5% to 15%) in the spectral region of high absorption of toluene. So, taking into account toluene consumption, $([OD]_{\lambda,RO_2})_0$ was calculated according to the following relation:

$$[OD]_0 = ([OD]_{\lambda,RO_2})_0 + ([\Delta OD]_{\lambda,tol})_0$$
$$([\Delta OD]_{\lambda,tol})_0 = \sigma_{\lambda,tol} \cdot l \cdot \Delta C_{tol} \quad (3b)$$

Here $[OD]_0$ is the apparent initial optical density and ΔC_{tol} represents the quantity of toluene lost via reaction with Cl atoms.

As stated in paragraph II.B, the experimental conditions were chosen to have a fast conversion of Cl atoms into RO_2. Therefore, ΔC_{tol} is equal to $[Cl^{\bullet}]_0$, which was obtained relative to the ethylperoxy radical ($[Cl^{\bullet}]_0 = [C_2H_5O_2]_0$). The values of $[OD]_0$ and $([OD]_{250,C_2H_5O_2})_0$ were determined by extrapolating to $t = 0$ the first points of the signal OD = f(t), immediately obtained after the laser pulse and for which the main absorbing species are RO_2 radical and toluene (see Figure 2a,b). The absorption of other species was neglected (reaction products).

It should be noted that, to be able to record the data during the formation of the peroxy radical and before the fast formation of the other absorbing species and thus to avoid a considerable loss of information near $t = 0$, the postflash dead time (time between the laser pulse and the information recording) was regulated at about 10 μs, the lowest value optimized in our experimental conditions. This possibility to get information near $t = 0$ differentiates the laser photolysis technique from the other techniques and shows its capacity to store data, especially in the case of fast reactions.

B. Factor Analysis (FA). Owing to the complexity of the reactive system (several species absorb in the same spectral region), we have used FA treatment to interpret the experimental optical density signals.

B.1. Reasons for Interest in FA Treatment. As mentioned in section III.A, the determination by the classical method of the cross section values of benzylperoxy radical is achieved by using only the first points of each signal, represented by the plot of the OD vs time for a specific wavelength.

In contrast, the FA method permits the simultaneous analysis of the curves obtained at different wavelengths and treats the whole signal for each curve. This treatment leads to more accurate results and allows us to validate and improve the values obtained by the classical method. Moreover, the FA method permits researchers to obtain further information such as the number and concentrations of the major absorbing species. This last point is a new and important element for simulation analysis.

B.2. Brief Description of FA Treatment. The literature concerning FA treatment is abundant. A good review on the subject is that by Malinowski.[16] This method is well adapted to the treatment of problems which follow the Beer−Lambert law, where the optical densities given by experiments can be written in matrix form:

$$\underset{r\times l}{\mathbf{D}} = \underset{r\times m}{\mathbf{C}} \cdot \underset{m\times l}{\mathbf{S}} + \underset{r\times l}{\mathbf{E}} \quad (4)$$

Here **D** is the $r \times l$ matrix of the experimental optical densities divided by the optical path for r times at l wavelengths. **C** is the $r \times m$ matrix of the "true" concentrations for m absorbing species, and **S** is the $m \times l$ matrix of the "true" spectra. **E** is the "true" $r \times l$ matrix of the errors.

The factor analysis method involves two main steps:

(a) Abstract Step. This part, called eigenanalyses, is purely mathematical, yielding matrixes of eigenvalues (Λ) and associated eigenvectors (Q) of the covariance matrix $\mathbf{Z} = \mathbf{D}'\cdot\mathbf{D}$ (where $'$ is the symbol of transposed matrix). It gives

$$\underset{r\times l}{\mathbf{D}^{++}} = \underset{r\times n}{\mathbf{C}_{abs}} \cdot \underset{n\times l}{\mathbf{S}_{abs}} \quad (5)$$

where $\mathbf{C}_{abs}$ and $\mathbf{S}_{abs}$ are the abstract matrixes of concentrations and spectra respectively for the n main absorbing species ($n \leq m$) (see Supporting Information). $\mathbf{D}^{++}$ represents the matrix of optical density reduced to the main components only. Likewise an important part of the error matrix **E** is suppressed and the remaining part is included in $\mathbf{D}^{++}$. So, this step eliminates an important part of the noise present in a whole series of experiments (experiments realized under given experimental conditions at different wavelengths) (see Figure 2) and reduces the study of this series of components to only the main factors.

(b) Transformation. The objective of this second step is to transform the abstract matrixes $\mathbf{C}_{abs}$ and $\mathbf{S}_{abs}$ to chemically recognizable factors. For this purpose, quite a few techniques are available. One of them is known as target transformation.[16] It allows the individual identification of the main factors. It necessitates having an initial test vector (target vector) $\mathbf{s_j}$ for each assumed absorbing factor from which a predicted vector $\hat{\mathbf{s}}_\mathbf{j}$ is calculated with its associated transformation vector $\mathbf{t_j}$ by a least-squares procedure. The comparison between the two vectors $\mathbf{s_j}$ and $\hat{\mathbf{s}}_\mathbf{j}$ permits validation of the hypothesis and produces better values for the cross sections of the hypothetical absorbing factors. In our study, this step confirms that the best test vectors (row vectors) are the RO_2 and R′CHO spectra previously measured. It is to be noted that, for the RO_2 radical, such determination is based on the whole experimental data and not only on the first points as done in the classical method. We can write

$$\underset{1\times l}{\hat{\mathbf{s}}_\mathbf{j}} = \underset{1\times n}{\mathbf{t_j}} \cdot \underset{n\times l}{\mathbf{S}_{abs}} \quad (6)$$

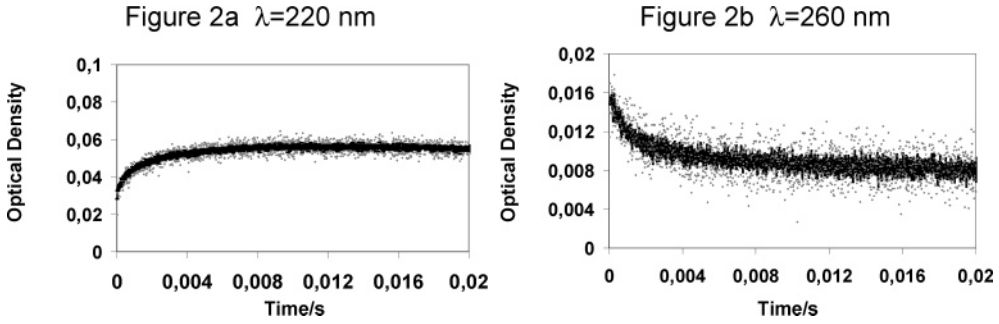

Figure 2. Comparison between optical density profiles obtained with the classical method (dotted line) and optical density profiles obtained after FA treatment (solid line). Experimental conditions: $T = 298$ K; $P = 102$ Torr; $[Cl_2]_0 = 3.10 \times 10^{15}$ molecule·cm^{-3}; $[\text{toluene}]_0 = 3.64 \times 10^{15}$ molecule·cm^{-3}.

TABLE 1: Reaction Scheme Used in the Simulation

reacn	rate const[a]	ref
$2C_6H_5CH_2O_2 \rightarrow 2C_6H_5CH_2O + O_2$ (Ia)	see text	this work
$2C_6H_5CH_2O_2 \rightarrow C_6H_5CHO + C_6H_5CH_2OH + O_2$ (Ib)	see text	this work
$2C_6H_5CH_2O_2 \rightarrow C_6H_5CH_2O_2CH_2C_6H_5 + O_2$ (Ic)	see text	this work
$C_6H_5CH_2O_2 + HO_2 \rightarrow C_6H_5CH_2O_2H + O_2$ (II)	see text	this work
$C_6H_5CH_2O_2CH_2C_6H_5 + M \rightarrow 2C_6H_5CH_2O + M$ (III)	8.00×10^{-11}	this work[b]
$C_6H_5CH_3 + Cl \rightarrow C_6H_5CH_2 + HCl$ (IV)	6.10×10^{-11}	11
$C_6H_5CH_2 + O_2 + M \rightarrow C_6H_5CH_2O_2 + M$ (V)	$7.60 \times 10^{-13}e^{191/T}$	19
$C_6H_5CH_2O + O_2 \rightarrow C_6H_5CHO + HO_2$ (VI)	$6.29 \times 10^{-14}e^{-507/T}$	c
$HO_2 + HO_2 \rightarrow H_2O_2 + O_2$ (VII)	$2.20 \times 10^{-13}e^{600/T}$	20
$CH_3OH + Cl \rightarrow CH_2OH + HCl$ (VIII)	5.50×10^{-11}	20
$CH_2OH + O_2 + M \rightarrow HO_2 + CH_2O + M$ (IX)	9.60×10^{-12}	20
$CH_2O + Cl \rightarrow CHO + HCl$ (X)	$8.10 \times 10^{-11}e^{-34/T}$	20
$CHO + O_2 + M \rightarrow HO_2 + CO + M$ (XI)	$3.49 \times 10^{-12}e^{140/T}$	15
$CH_2OH + HO_2 \rightarrow CH_2O + H_2O_2$ (XII)	2.00×10^{-11}	21
$CH_2OH + Cl \rightarrow CH_2O + HCl$ (XIII)	6.64×10^{-10}	22

[a] cm^3 molecule^{-1} s^{-1} for bimolecular reaction and s^{-1} for unimolecular reaction. [b] Estimated value. [c] Comparable to the reaction of CH_3CH_2O with O_2.[15]

where $\hat{\mathbf{s}}_\mathbf{j}$ and $\mathbf{t}_\mathbf{j}$ are row vectors and **j** successively takes the values 1 to *n*.

At the end of this process, we obtain

$$\underset{r\times l}{\mathbf{D}^{++}} = \underset{r\times n}{\mathbf{C}_{abs}}\cdot\underset{n\times l}{\mathbf{S}_{abs}} = \underset{r\times n}{\mathbf{C}_{abs}}\cdot\underset{n\times n}{\mathbf{T}^{-1}}\cdot\underset{n\times l}{\mathbf{T}}\cdot\underset{n\times l}{\mathbf{S}_{abs}} = \underset{r\times n}{\hat{\mathbf{C}}}\cdot\underset{n\times l}{\hat{\mathbf{S}}} \qquad (7)$$

where $\hat{\mathbf{S}}$ is the matrix of the spectra recalculated using all the data of a series of experiments (typically 7−13 wavelengths over 0.02 s by step of 10^{-5} s) and $\hat{\mathbf{C}}$ is the matrix of the individual concentrations of the main absorbers. It is important to note that this last piece of information is specific to FA analysis and is important for the simulation phase.

C. Kinetic Determinations of the Benzylperoxy Radical Self-Reaction and of Its Reaction with HO_2. Due to the complex nature of the chemical system, our experiments were simulated to extract the kinetic parameters of reactions I and II. To obtain more credible simulation results, quite a large range of experimental conditions were used; in particular, we modified the initial total concentrations (molecule·cm^{-3}) of RO_2 and HO_2 from 1×10^{13} to 1×10^{14} and the ratio τ = methanol/toluene from 0 to 2. These modifications were obtained by varying the chlorine, toluene, and methanol concentrations and the laser energy. The reaction scheme used is presented in Table 1. This kinetic model uses the main processes occurring during the photolysis of the mixture ($Cl_2/C_6H_5CH_3/CH_3OH/O_2/N_2$). It includes reactions producing and consuming $C_6H_5CH_2O_2$ and HO_2.

The computed optical densities include the absorption of the following species: $C_6H_5CH_2O_2$, HO_2, H_2O_2, $C_6H_5CH_2O_2H$, C_6H_5CHO, $C_6H_5CH_2OH$, and $C_6H_5CH_3$. The $C_6H_5CH_2OH$ spectrum was determined in our laboratory. The absorption cross section values of $C_6H_5CH_2O_2$ are those derived from this study. For HO_2 and H_2O_2, the absorption cross-section values are those recommended by DeMore et al.[15] The cross sections of $C_6H_5CH_2O_2H$ were set equal to that of $ClCH_2CH_2O_2H$ recommended by Chakir et al.[13] The C_6H_5CHO spectrum was determined in our laboratory and in LCSR Orléans, with good accuracy in separate experiments using two different systems (D_2 lamp−diode array and D_2 lamp−monochromator).[17] The consumption of toluene was also taken into account in the computed optical densities. Table 2 summarizes the cross-section values used in the simulation. The kinetic parameters employed were taken from the literature except for those of reactions Ia, Ib, Ic, and II. The k_I and k_{II} values were obtained by simulating the time-dependent OD profiles at different wavelengths and the time−concentration profiles of the main absorbing species extracted by FA treatment. During the simulation, the rate constants of reactions I and II were varied until the best agreement was obtained between the simulation and the experimental data (the difference between the computed optical densities and the experimental ones does not exceed 10%).

IV. Results

A. Data Exploitation.

A.1 Classical Method: Cross sections σ_{λ,RO_2} determination. Cross-section values of $C_6H_5CH_2O_2$ between 220 and 280 nm, obtained from the curves OD = f(*t*) as described in section III.A, are listed in Table 2. To reduce error, several experiments were carried out at each wavelength and yielded an average σ_{λ,RO_2} for which the quoted errors were the standard deviation.

As cited above, these values were obtained relative to the absorption cross section of the $CH_3CH_2O_2$ at 250 nm. In the

TABLE 2: Absorption Cross Section Values Used in Kinetic Analysis for Benzyl Peroxy Radical and Other Absorbing Species

	$10^{-18}\sigma_\lambda$ (cm^2·molecule^{-1})				
λ (nm)	$C_6H_5CH_2O_2$[a]	$C_6H_5CH_2O_2$[b]	C_6H_5CHO	$C_6H_5CH_2OH$	$C_6H_5CH_3$
220	6.70 ± 1.20	8.20 ± 0.40	21.0 ± 2.00	0.045 ± 0.007	0.263 ± 0.06
225	5.60 ± 1.70	6.60 ± 0.25	32.0 ± 2.40	0.053 ± 0.006	0.034 ± 0.007
230	5.00 ± 0.60	5.30 ± 0.15	39.0 ± 3.00	0.07 ± 0.009	0.041 ± 0.007
235	4.70 ± 0.60	5.10 ± 0.35	32.0 ± 2.80	0.072 ± 0.009	0.076 ± 0.009
240	4.90 ± 0.70	5.00 ± 0.40	24.0 ± 2.10	0.063 ± 0.008	0.142 ± 0.02
245	5.00 ± 0.65	5.30 ± 0.20	2.08 ± 0.30	0.024 ± 0.009	0.240 ± 0.002
250	4.80 ± 0.40	4.70 ± 0.20	1.30 ± 0.30	0.02 ± 0.005	0.324 ± 0.03
255	3.90 ± 0.80	4.30 ± 0.20	0.92 ± 0.14	0.019 ± 0.004	0.446 ± 0.03
260	3.80 ± 0.50	3.90 ± 0.20	1.25 ± 0.25	0.023 ± 0.005	0.531 ± 0.03
265	2.50 ± 0.50	2.60 ± 0.20	1.75 ± 0.30	0.025 ± 0.006	0.364 ± 0.003
270	2.25 ± 0.30	2.25 ± 0.10	2.11 ± 0.30	0.023 ± 0.005	0.142 ± 0.015
275	1.70 ± 0.20	1.90 ± 0.10	3.79 ± 0.60	0.024 ± 0.004	0.022 ± 0.003
280	1.70 ± 0.20	1.60 ± 0.10	1.79 ± 0.30	0.023 ± 0.004	0.003 ± 0.0004

[a] $C_6H_5CH_2O_2$ cross sections obtained by the classical method. [b] $C_6H_5CH_2O_2$ cross sections obtained by the FA method.

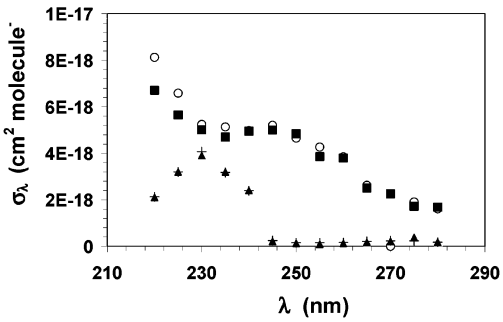

Figure 3. $C_6H_5CH_2O_2$ and C_6H_5CHO spectra. (The spectra of C_6H_5-CHO are divided by a factor of 10). Key: (○) $C_6H_5CH_2O_2$ spectrum determined by FA treatment; (■) $C_6H_5CH_2O_2$ spectrum determined by the classical method; (+) C_6H_5CHO spectrum determined by FA treatment; (▲) C_6H_5CHO spectrum determined by Thiault et al.[17]

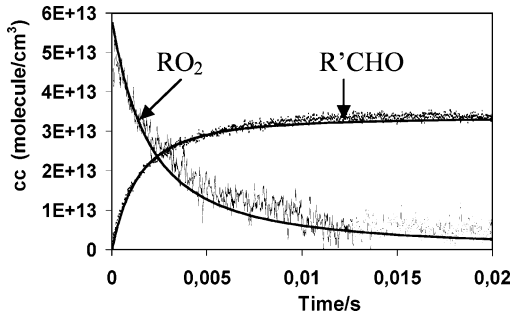

Figure 4. Concentration profiles of C_6H_5CHO and $C_6H_5CH_2O_2$ obtained by factor analysis method and by simulation. Experimental conditions: $T = 298$ K; $P = 101$ Torr; $[Cl_2]_0 = 3.90 \times 10^{15}$ molecule·cm^{-3}; $[\text{toluene}]_0 = 2.90 \times 10^{15}$ molecule·cm^{-3}.

wavelength range 220−240 nm, some species strongly absorb, and this affects the measurements and the extraction of the initial optical density of $C_6H_5CH_2O_2$ and causes high quoted error limits. The uncertainty in the cross sections may exceed 20%.

Between 245 and 260 nm, the RO_2 absorbs a lot in comparison with the other absorbing species. The cross-section values in this region were obtained with good accuracy.

In the wavelength range 270−280 nm, where the $C_6H_5CH_2O_2$ absorption is weak, the cross-section uncertainties can increase up to 15%.

Figure 3 shows the spectrum of RO_2 obtained relative to the absorption cross section of $CH_3CH_2O_2$ at 250 nm. As can be seen, the UV absorption spectrum of this radical consists of a broad continuum and shows two bands of absorption. The first one, with a maximum between 240 and 245 nm, characterizes the COO chromophore. The second one, located below 225 nm, could be attributed to the presence of the aromatic group.

A.2. Factor Analysis Method. A.2.1. Step 1:

Determination of the number of major absorbing species. Different statistical tests (see Supporting Information) were used in this work to determine the number of significant species. The results show that there are two important factors to reproduce the experimental data. These two factors have been easily identified as RO_2 and R′CHO (see next section). As cited in section III.B.2, this step eliminates a major part of the noise in the signals, mainly in the noisy absorption region above 260 nm, as shown in Figure 2.

A.2.2. Step 2:

Determination of the major absorbing species cross sections and concentrations. Figure 3 compares the spectra determined by FA treatment and those obtained by the classical method for RO_2 (target spectra) and given by Thiault et al.[17] for R′CHO. The discrepancy was found to not exceed 10%.

The concentrations of the major absorbing species (RO_2 and R′CHO) have been extracted by factor analysis at $T = 298$ K.

The concentration profiles of RO_2 and R′CHO are given in Figure 4. It is to be noted that these data are obtained without any hypothesis on the kinetic mechanism.

B. Data Simulation.

B.1. Self-Reaction of $C_6H_5CH_2O_2$ Radicals. The rate constants were determined by analyzing the following:

(i) Temporal profiles of optical density obtained in the spectral region 245−255 nm where the benzylperoxy radical absorption is important. The precision of the experimental data in this spectral region was the best, owing to the very small absorption of HO_2 and benzaldehyde which did not affect the absorption shape of benzylperoxy radical. The signals obtained in the region 220−240 nm and above 255 nm were used to validate the determinations obtained in the spectral region 245−255 nm.

(ii) Concentration profiles of RO_2 and R′CHO determined by factor analysis. The experimental conditions were widely varied and were chosen to avoid secondary reactions (conditions for which the concentration of $C_6H_5CH_2O_2$ does not exceed 1×10^{14} molecule·cm^{-3} and the reaction time does not exceed a few milliseconds). In such conditions, the reaction mechanism (Table 1) composed by reactions I−XIII appears to describe the reactive system studied in this section.

The values of k_I determined at different temperatures are listed in Table 3. As it can be seen, there is a slight variation of the k_I value with temperature. The following Arrhenius expression

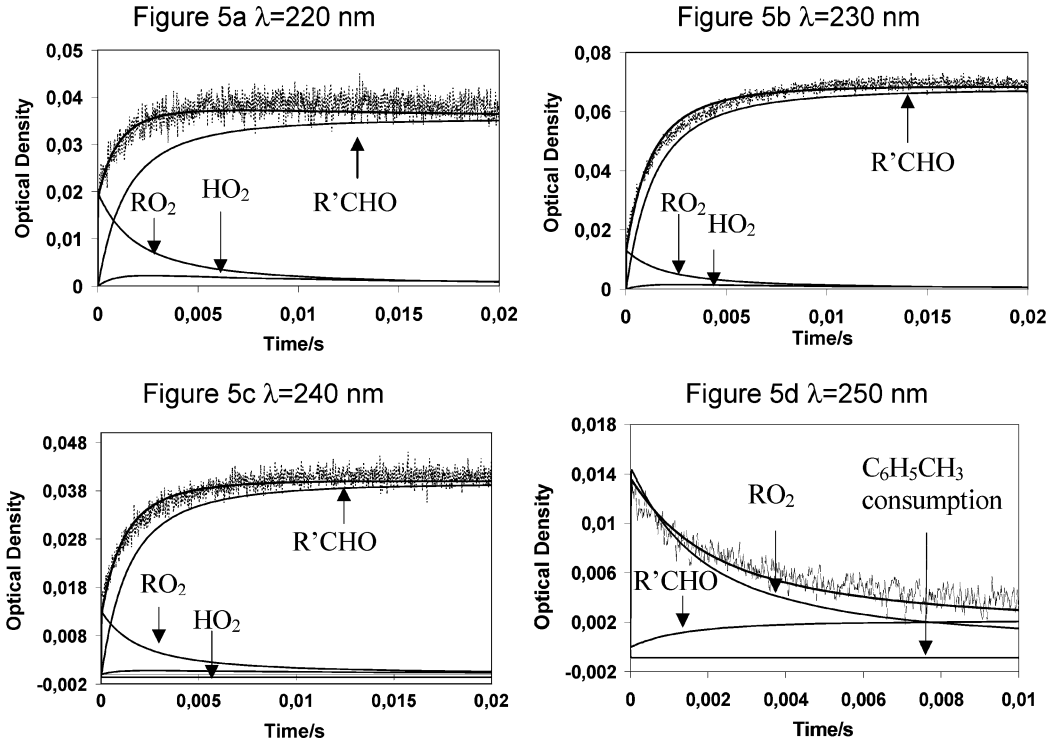

Figure 5. Optical density versus time: Confrontation model-experiment for $T = 298$ K, $P = 101$ Torr, $[Cl_2]_0 = 3.90 \times 10^{15}$ molecule·cm^{-3}, and $[\text{toluene}]_0 = 2.90 \times 10^{15}$ molecule·cm^{-3}.

TABLE 3: k_I, k_{Ic}, and Branching Ratio as a Function of Temperature

T (K)	$10^{12}k_I$ (molecule^{-1}·cm^3·s^{-1})	$\alpha = k_{Ia}/k_I$	$\delta = k_{Ic}/k_I$	no. of experiments
298	4.20 ± 0.70[a]	0.44	0.20	12
313	3.80 ± 0.60	0.45	0.14	8
323	3.40 ± 0.40	0.46	0.12	8
333	3.00 ± 0.40	0.46	0.08	8
343	2.33 ± 0.30	0.46	0.07	8
353	1.83 ± 0.30	0.45	0.09	8

[a] Standard deviation.

of k_I between 298 and 353 K is obtained using a least-squares fitting:

$$k_I = 2.50 \times 10^{-14} \exp(1562/T) \text{ molecule}^{-1}\cdot\text{cm}^3\cdot\text{s}^{-1}$$

To simulate our experiments correctly, whatever the wavelength, the branching ratio ($\alpha = k_{Ia}/k_I$) was varied between 0.44 and 0.5 (interval recommended by Nozière et al.)[11] and k_{Ic} between 8 and 20% of k_I . The best fitted values of k_{Ia}/k_I and k_{Ic}/k_I are presented in Table 3. Some results of the simulation are shown in Figure 5a−d. As can be seen, the simulation reproduces the experimental data quite well and confirms the credibility of the determined kinetic parameters and of the reaction scheme chosen.

B.2. Reaction of $C_6H_5CH_2O_2$ with HO_2. Transition absorption profiles were recorded at wavelengths 225 and 250 nm following the pulsed photolysis of the ($Cl_2/C_6H_5CH_3/CH_3OH/O_2/N_2$) mixture. To extract the kinetic parameters of reaction II correctly, several experiments were carried out at various HO_2 and RO_2 concentrations obtained by varying the toluene and methanol concentrations. At 250 nm, where the absorption of benzylperoxy radical is important, it was observed that the total absorption decreases with time. However, at 225 nm, the absorption of HO_2 and the benzylperoxy radicals are of the same magnitude, and therefore the form of the signal depends on τ (the ratio of methanol to toluene). In fact, when τ is less than 2, benzaldehyde, the main stable product formed during the experiments, strongly absorbs and completely hides the evolution of HO_2 and benzylperoxy radicals. Thus, the signal obtained increases with time. On the other hand, when τ is greater or equal to 2, the concentration of HO_2 is important and therefore slows down the formation of benzaldehyde by trapping the benzylperoxy radicals via reaction II. In this case, the optical density curves decrease with time.

TABLE 4: k_{II} as a Function of Temperature

T (K)	$10^{12}k_{II}$ (molecule^{-1}·cm^3·s^{-1})	no. of experiments
298	12.50 ± 2.00	12
313	11.10 ± 2.00	12
323	9.70 ± 2.00	12
333	8.30 ± 1.20	12
343	6.20 ± 1.20	12
353	5.50 ± 1.40	12

The kinetic analyses of these different signals, using the mechanism presented in Table 1, yield the kinetic parameters of reaction II. The values of k_{II}, at different temperatures, are listed in Table 4. The linear least-squares fitting leads to the Arrhenius expression

$$k_{II} = 5.70 \times 10^{-14} \exp(1649/T) \text{ molecule}^{-1}\cdot\text{cm}^3\cdot\text{s}^{-1}$$

Some results of the simulation-experiment similarity are shown in Figures 6 and 7.

V. Discussion

A. Reaction Mechanism. The mechanism of peroxy radical self-reaction has been studied extensively.[6−9] Three reaction pathways are generally considered (reactions Ia, Ib, and Ic in Table 1). Reaction pathway (Ic) has never been characterized clearly. The kinetic study of RO_2 achieved by Nozière et al.,[11] using two detection techniques (FTIR and UV spectroscopy),

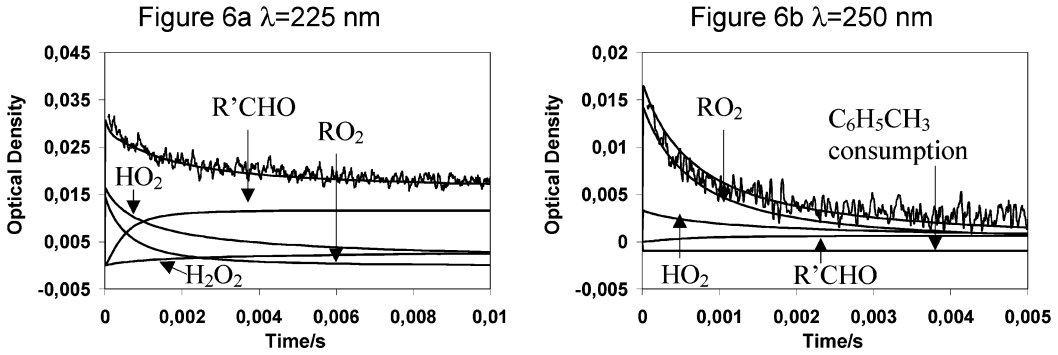

Figure 6. Optical density versus time: Confrontation model-experiment for $T = 298$ K, $P = 102$ Torr, $[Cl_2]_0 = 3.00 \times 10^{15}$ molecule·cm^{-3}, $[\text{toluene}]_0 = 3.30 \times 10^{15}$ molecule·cm^{-3}, and $[CH_3OH] = 6.60 \times 10^{15}$ molecule·cm^{-3}.

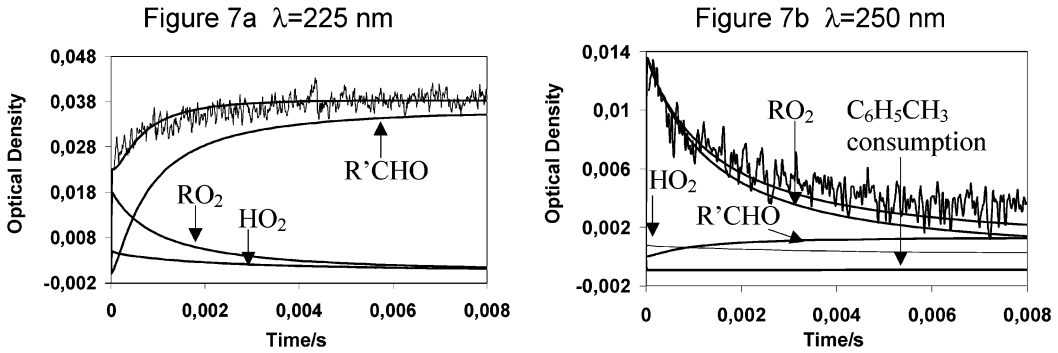

Figure 7. Optical density versus time: Confrontation model-experiment for $T = 298$ K, $P = 100$ Torr, $[Cl_2]_0 = 5.00 \times 10^{15}$ molecule·cm^{-3}, $[\text{toluene}]_0 = 2.40 \times 10^{15}$ molecule·cm^{-3}, and $[CH_3OH] = 1.15 \times 10^{15}$ molecule·cm^{-3}.

shows a molar product yield for R′CHO of about 45% and a deficit in the carbon balance of about 20% attributed to the peroxide RO_2R. In our work, the FA technique gives a direct measurement (without hypothesis on the kinetic scheme) of the RO_2 and R′CHO concentrations. Our results show that the benzaldehyde yield, calculated relative to the initial concentration of benzylperoxy radical, is about (65 ± 5)%. This result is in disagreement with the literature (Nozière et al.[11]). Our results can be compared to those obtained by Nozière et al.[11] only in its UV spectroscopy analysis. This discrepancy is not mechanistic but is mainly due to the cross-section values of R′CHO and RO_2 used in the calculations. The spectrum of R′CHO has recently been reinvestigated in our laboratory and in LCSR Orléans using two different experimental systems.[17] The results obtained are in accordance with the recent data of Etzkorn et al.[18] and therefore are certainly more accurate than the data of ref 11. Therefore, if the yield value of C_6H_5CHO obtained by Nozière et al.[11] using flash photolysis technique (45%) is corrected by the appropriate coefficient, $(\sigma_{R'CHO}/\sigma_{RO_2})_{(11)} \times (\sigma_{RO_2}/\sigma_{R'CHO})_{\text{this work}} = 1.5$, one obtains 68% as the molar product yield of C_6H_5CHO, which is in very good accordance with ours (65 ± 5)%.

To improve the simulation fit and to obtain very accurate values, especially at low wavelengths, where the absorption is mainly due to the benzaldehyde, we added to our kinetic scheme the reaction of decomposition of the unstable product RO_2R,

$$\text{M: ROOR} + \text{M} \rightarrow 2\text{RO} + \text{M} \qquad \text{(III)}$$

and we varied the branching ratio (α) between 0.44 and 0.5 (interval recommended by ref 11).

Concerning the reaction of RO_2 with HO_2, it proceeds mainly via the channel

$$RO_2 + HO_2 \rightarrow \text{ROOH} + O_2 \qquad \text{(II)}$$

to produce ROOH.[6−9] As it is explained in section IV.B.2, the kinetic parameters of this reaction were extracted by simulating several optical density signals obtained at various experimental conditions.

B. Evaluation of the Errors. Random errors are easily dealt with by repeating the experiments. Systematic errors are the main sources of errors and therefore have to be hunted down. The first section explains how to reduce the noise associated with random errors studied by the factor analysis technique. The second section explains the origins of systematic errors.

B.1. Random Error. This error is studied in the context of factor analysis and presented in details in the literature.[16] Therefore, it will be briefly described here.

Because of experimental errors, the optical densities d_{ik} are simply the sum of two terms:

$$d_{ik} = d_{ik}^* + e_{ik} \qquad (8)$$

Here $i = 1$ to r and $k = 1$ to l (r and l represent time and wavelengths respectively), d_{ik}^* represents the pure optical density, and e_{ik} is the experimental error. This last term cannot be completely extracted by factor analysis, and a part of error remains in the optical density values obtained by FA. Therefore, the experimental error e_{ik} can be written as a sum of two terms:

$$e_{ik} = e_{ik}^{++} + e_{ik}^{0} \qquad (9)$$

Here e_{ik}^0 is the part of error removed by deleting the unnecessary eigenvectors and e_{ik}^{++} is the part of error included in the optical densities d_{ik}^{++}. So

$$d_{ik} = d_{ik}^{++} + e_{ik}^{0} \qquad (10)$$

where $d_{ik}^{++} = d_{ik}^* + e_{ik}^{++}$.

In our case, because of the reduction of the data to two main absorbing species, RO_2 and R′CHO, instead of six (RO_2, R′CHO, ROH, ROOH, HO_2, H_2O_2) (the variation due to RH was initially removed from OD), the optical densities extracted by factor analysis (d_{ik}^{++}) are affected not only by a "true" random error e_{ik}^{++} but also slightly by the absorption of the minor species.

B.2. Systematic Errors.

UV spectrum of the benzylperoxy radical. As described above, in the classical method, benzylperoxy radical cross sections σ_λ were determined relative to σ_{250}, the cross section of ethylperoxy radical at 250 nm and by extrapolating the signal to $t = 0$ to optimize initial optical densities. The ethylperoxy radical cross section used is given by Tyndall et al.[9] with 5% relative uncertainty. The initial absorbance was optimized, using the nonlinear least-squares fitting to fit the first points of the signal obtained just after the laser pulse. In the spectral range 245−265 nm, where the initial optical density of the peroxy radical is not affected by the product absorbance, the uncertainty on the cross section does not exceed 15%. However, in the spectral range 220−245 nm, the absorption of the products, mainly the benzaldehyde, is very strong and therefore affects the initial absorbance of RO_2. The same remark can be made above 265 nm, where the peroxy radical and the benzaldehyde absorbances are of the same magnitude. In these spectral regions (below 245 and above 265 nm), the estimated total error may reach 30%.

As cited above, the FA method eliminates part of random error on the signals. Therefore, the uncertainty on the RO_2 cross-section values obtained using this method was found to not exceed 15% over the entire spectral range.

Rate Constants k_I and k_{II}. Using several experimental conditions, for which the sensibilities of reactions I and II were varied relative to each other, their kinetic parameters were simultaneously determined. The sources of uncertainty in the determination of rate constants k_I and k_{II} are mainly due to the following:

(i) Initial reagent concentrations and the stability of the laser energy. To simulate our experiments with good accuracy, it is necessary to know the initial chlorine atom concentration and the ratio τ (methanol/toluene) exactly. In each experiment, $[Cl]_0$ was determined relative to the ethylperoxy radical concentration: $[Cl]_0 = [C_2H_5O_2]_0 = [C_6H_5CH_2O_2]_0 + [HO_2]_0$ with $[HO_2]_0$ equal to 0 when $\tau = 0$. This relation is valid if the initial molecular chlorine concentration is constant. This constancy depends mainly on the stability of the laser energy during the experiment. The initial chlorine, toluene, and methanol concentrations and the laser energy were determined before and after each experiment, and the variations were less than 5% and 1% respectively for initial concentrations and laser energy. The uncertainty of the initial chlorine atom concentration and that of the ratio τ are approximately 10%. These uncertainties imply contributions of respectively 10% and 15% on the total error in k_I and k_{II}.

(ii) Reaction scheme used to reproduce our experiments and to extract the kinetic parameters. This model was established as follows. First, on the basis of the results found in the literature concerning the same reactive systems, we developed a reaction mechanism including all the reactions susceptible to be produced during the experiment. Second, to identify the rate-determining steps in the mechanism scheme, sensitivity analyses on the computed results were carried out. The results show that the main sensitive reaction steps are those listed in Table 1, whose kinetic data are well-known except for reactions I and II.

(iii) Effect of α and δ. As noted in Table 3, branching ratios $\alpha = k_{Ia}/k_I$ and $\delta = k_{Ic}/k_I$ are as follows: $0.44 \leq \alpha \leq 0.50$ (interval recommended by ref 11) and $0.08 \leq \delta \leq 0.20$. The effects of α and δ were simultaneously studied at different ratios τ (methanol/toluene) ranging from 0 to 2. The sensitivity analyses showed that α depends significantly on τ, and the effect of α on the rate constants is mainly noticed in the case of $\tau = 0.5$. In fact, a variation in α of about 15% at 225 nm implies uncertainties of respectively 5%, 7%, and 12% for $\tau = 2$, $\tau = 1$, and $\tau = 0.5$ in k_{II}, whereas a variation of 15% on δ implies uncertainties in k_{II} of about 2%.

The above observations may be explained as follows: channel (Ia), whose branching ratio is α, is a nontermination channel and yields the benzaldehyde, which is the main absorbing species at 225 nm and defines the form of the signal, mainly at $\tau = 0.5$ where it is in high concentration.

In addition, sensitivity analysis showed that the k_{II} values are more sensitive to perturbations on α at 225 nm than at 250 nm regardless of τ (0.5, 1, 2). In fact, a perturbation of 15% on α implies uncertainties less than 2% on the k_{II} value at 250 nm. The effect of δ is less important than that of α, and uncertainties on δ do not affect the computed optical density significantly.

(iv) Cross Section Values. As indicated in section III.C, the computed optical densities take into account the absorption of the following species: $C_6H_5CH_2O_2$, HO_2, H_2O_2, $C_6H_5CH_2O_2H$, C_6H_5CHO, $C_6H_5CH_2OH$, and $CH_3C_6H_5$. The sensitivity analyses show that the cross-section values of H_2O_2, $C_6H_5CH_2O_2H$, and $C_6H_5CH_2OH$ are of negligible effect on the simulation results. A perturbation of 50% on these parameters implies a contribution of less than 5% on the total error in k_I and k_{II}. However, the contribution of the HO_2 cross section becomes quite significant below 230 nm and in the experimental conditions for which the HO_2 influence is not completely hidden by the benzaldehyde absorption ($\tau > 1$). The individual uncertainty due to the HO_2 cross-section values does not exceed respectively 5% and 10% in the total error of k_I and k_{II}. On the other hand, the uncertainty induced by the benzaldehyde absorption cross-section values is very high at wavelengths lower than 245 nm. At 250 nm, the relative uncertainty of the benzaldehyde absorption cross-section values is about 15%, and this uncertainty implies contributions of respectively 5% and 15% on the total error in k_I and k_{II}. Finally, because the principal parameter leading to errors in k_I and k_{II} is the absorption cross-section value of $C_6H_5CH_2O_2$, repeated measurements were performed mainly at 250 nm. The error, estimated to 15%, implies contributions of respectively 10% and 15% on the total error in k_I and k_{II}.

In light of the explanations above, to extract kinetic parameters, the simulation was carried out in the spectral range 245−255 nm where the error is minimized. The other spectral regions were used to validate kinetic determinations and also to optimize the branching ratio. The total uncertainties in k_I and k_{II} are approximately 25% and 45%, respectively.

C. Comparison with previous studies.

Cross section values. Only one determination of the UV spectrum of the $C_6H_5CH_2O_2$ radical is available in the literature.[11] Figure 8 compares the values of the absorption cross sections determined in this work with the literature,[11] the experimental technique used in the literature[11] being the flash photolysis. Below 240 nm, our values are close to those obtained by Nozière et al.[11] with a difference less than 10%. In the spectral range 240−280 nm, the values obtained by Nozière et al.[11] are higher than ours and the discrepancy exceeds 30%. As described by Nozière et al.,[11] the postflash dead time used in

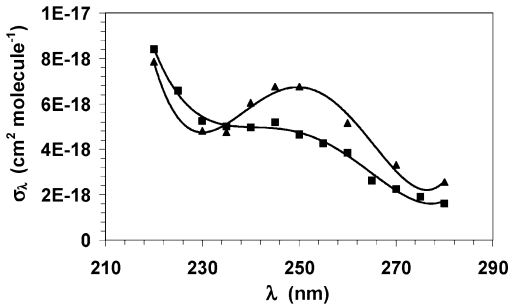

Figure 8. $C_6H_5CH_2O_2$ spectrum obtained in this work compared with the literature: (■) $C_6H_5CH_2O_2$ spectrum determined in this work using the FA method; (▲) $C_6H_5CH_2O_2$ spectrum determined by Nozière et al.[11]

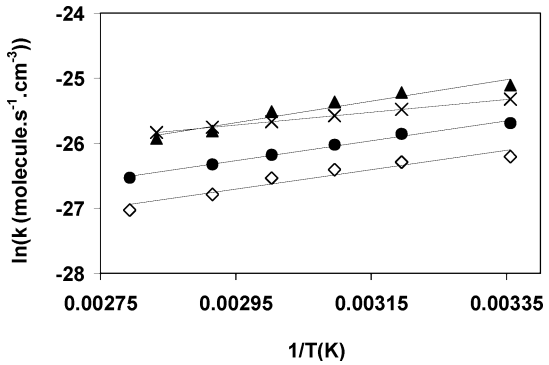

Figure 9. Arrhenius plot for k_I and k_{II}: (◇) k_I determined in this work; (●) k_I determined by Nozière et al;[11] (▲) k_{II} determined in this work; (×) k_{II} determined by Nozière et al.[11]

their study (about 250 μs, time for which the formation of benzaldehyde is relatively important) can affect the determination of the initial optical densities and explain why the values obtained by Nozière et al.[11] are overestimated.

k_I and k_{II} values. A comparison between rate constants k_I and k_{II} obtained in this study and those found in the literature[11] is illustrated in Figure 9.

The k_I values determined by Nozière et al.[11] are 40−65% greater than ours. More than 40% of this discrepancy originates from the cross-section values of benzaldehyde used in the calculation. In fact, the benzaldehyde cross-section values obtained by Nozière et al.[11] in the spectral range 250−260 nm are 2−3 times larger than ours and those found in the literature.[17,18] The second source of the discrepancy is given by the cross-section values of the benzylperoxy radical used at 250 nm.

In this study, the branching ratio used and the k_{Ic} value obtained at 298 K are close to those given by Nozière et al.[11] However, above 323 K, our k_{Ic} values are twice as low as those recommended by Nozière et al.[11] The determination of k_{II} at 250 nm depends mainly on σ_{250,RO_2} and the k_I value. In our work, the k_I and σ_{250,RO_2} values used are 40% to 65% and 40%, respectively, lower than those used by Nozière et al.[11] In the calculation of the optical density, the k_I discrepancy can be corrected by that of σ_{250,RO_2} and vice versa. Consequently, despite these large discrepancies, the k_{II} values obtained in this work are close to those determined by Nozière et al.[11] (The discrepancy does not exceed 20%.)

For both studies, k_I and k_{II} exhibit a negative temperature coefficient which confirms that reactions I and II proceed via the reversible formation of the intermediate tetroxides C_6H_5-$CH_2O_4CH_2C_6H_5$ and $C_6H_5CH_2O_4H$, respectively.

D. Effects of the Aromatic Group in the Peroxy Radical Structure.

UV spectrum. The comparison between the benzylperoxy radical and other primary peroxy radicals shows that their UV absorption spectra are similar in shape with a broad unstructured band in the 225−280 nm region, and their cross section values are of the same magnitude. However, in the benzylperoxy radical UV spectrum, an absorption band located below 225 nm was observed. This band is attributed to the presence of the aromatic ring in the radical structure revealing the effect of the aromatic group on the peroxy radical UV absorption.

Kinetic Parameters. Concerning the self-reaction, the comparison between the $C_6H_5CH_2O_2$ and the $CH_3CH_2O_2$ rate constants shows that the substitution of the methyl group in the ethylperoxy radical by an aromatic group in β position results in a significant increase in the self-reaction rate constant. The same remark could be noticed in previous work in our laboratory concerning other primary peroxy radicals, in particular $(CH_3)_2C$-$(OH)CH_2O_2$[14] and $ClCH_2CH_2O_2$.[13] In addition, the comparison between $C_6H_5CH_2O_2$, $ClCH_2CH_2O_2$, and $(CH_3)_2C(OH)CH_2O_2$ self-reactions reveals that the rate constants of the self-reactions are all in the same order of magnitude at 298 K and were found to display negative temperature dependence.

However, concerning the cross reaction with HO_2, as it was previously reported,[7,8,14] there is no clear influence of the β functional group nature on the reactivity, in particular of the aromatic group studied in this work. In fact, this cross-reaction rate constant is of the same order of magnitude as the rate constants for other peroxy radical cross reactions. The negative temperature dependence obtained for this reaction is comparable to those observed for other peroxy radicals and could be evidence for the existence of an intermediate complex as in the case of the self-reaction.

VI. Conclusion

In this work, the spectroscopic and the kinetic behavior of the benzylperoxy radical was studied using the pulsed laser photolysis technique. The UV spectrum of RO_2 was determined in the spectral region 220−280 nm using two different methods: the "classical method" and, for the first time in this type of studies, the "factor analysis method". The absorption maximum is located between 240 and 245 nm. The self-reaction and the cross reaction with HO_2 were studied over the temperature range 298−353 K, and kinetic parameters were determined. Moreover, the number and the concentration profiles of the main absorbing species were determined by using the FA method. Several conclusions can be drawn from these determinations. The UV spectrum of the benzylperoxy radical is similar in shape and magnitude to primary peroxy radical spectra in the spectral range 225−280 nm. The two rate constants found in this work present a negative temperature coefficient confirming the existence of intermediate adducts. It can be concluded by comparing these rate constants with those of primary peroxy β substituted radicals that the aromatic group does not bring any specificity in the reactivity of the radical. The comparison between our determinations and the only study found in the literature[11] concerning this radical shows that the discrepancy varies from 5% to 40% for the spectrum of RO_2. This may result from the difference in the ability of the techniques used in the two studies to measure the initial part of the signals. In addition, a comparison between kinetic parameters k_I and k_{II} obtained in this work and the only study available in the literature[11] shows a discrepancy of about 40−65% and 6−20% for k_I and k_{II}, respectively. These discrepancies originate

mainly from the cross-section values of the absorbing species (C_6H_5CHO, $C_6H_5CH_2O_2$) used in the calculation.

Acknowledgment. This work was supported by the "Region Champagne Ardenne" and the CNRS through the PNCA (Programme National de Chimie Atmosphérique) for which we are grateful.

Supporting Information Available: It contains details about the statistical tests used in FA treatment and results are summarized in Table (1S) and presented in Figure (1S). This material is available free of charge via the Internet at http://pubs.acs.org.

References and Notes

(1) Piccot, S. D.; Watson, J. J.; Jones, J. W. *J. Geophys. Res.* **1992**, *97*, 9897.

(2) Dearth, M. A.; Glerczak, C. C.; Siegl, W. O. *Environ. Sci. Technol.* **1992**, *26*, 1573.

(3) Westerholm, R.; Almén, J.; Li, H.; Rannung, U.; Rosén, A. *Atmos. Environ.* **1992**, *26B*, 79.

(4) Becker, K. H. The atmospheric oxidation of aromatic hydrocarbons and its impact on photooxidant chemistry. In *Proceedings of EUROTRAC Symposium*, 94th ed.; Borell, P. M., et al., Eds.; SPB Academic Publishing BV: The Hague; pp 67−74.

(5) Calvert, J. G.; Atkinson, R.; Becker, K. H.; Kamens R. M.; Seinfeld, J. H.; Wallington, T. J.; Yarwood, G. *The mechanisms of atmospheric oxidation of aromatic hydrocarbons*; Oxford University Press: New York, 2002.

(6) Lightfoot, P. D.; Cox, R. A.; Crowley, J. N.; Destriau, M.; Hayman, G. D.; Jenkin, M. E.; Moortgat, G. K.; Zabel, F. *Atmos. Environ.* **1992**, *26A*, 1805.

(7) Wallington, T. J.; Dagaut, P.; Kurylo, M. J. *Chem. Rev.* **1992**, *92*, 667.

(8) Lesclaux, R. *Peroxy Radicals*; Alfassi, Z. B., Ed.; John Wiley & Sons: New York, 1997.

(9) Tyndall, G. S.; Cox, R. A.; Granier, C.; Lesclaux, R.; Moortgat, G. K.; Pilling, M. J.; Ravishankara, A. R.; Wallington, T. J. *J. Geophys. Res.* **2001**, *106*, 12157.

(10) Derwent, R. G.; Jenkin, M. E. *Hydrocarbon Involvement in photochemical Ozone Formation in Europe*; Harwell Report, AERE-R 13736; AERE Harwell: Oxon, England, 1999.

(11) Nozière, B.; Lesclaux, R.; Hurley, M. D.; Dearth, M. A.; Wallington, T. J. *J. Phys. Chem.* **1994**, *98*, 2864.

(12) Fauvet, S.; Ganne, J. P.; Brion, J.; Daumont, D.; Malicet, J.; Chakir, A. *J. Chim. Phys*. **1997**, *94*, 484.

(13) Chakir, A.; Ganne, J. P.; Daumont, D.; Brion, J. *Phys. Chem. Chem. Phys.* **2003**, *5*, 2573−2580.

(14) Chakir, A.; Ganne, J. P.; Roth, E.; Brion, J.; Daumont, D. *Phys. Chem. Chem. Phys.* **2004**, *13*, 3383−3388

(15) DeMore, W. B.; Sander, S. P.; Golden, D. M.; Hampson, R. F.; Kurylo, M. J.; Howard, C. J.; Kolb, C. E.; Ravishankara, A. R.; Molina, M. J. *Chemical kinetics and photochemical data for use in stratospheric modelling*; NASA-JPL Publication, 97-4; NASA-JPL: Pasadena, CA, 1997.

(16) Malinowski, E. R. *Factor Analysis in Chemistry*, 3rd ed.; John Wiley & Sons: New York, 1991.

(17) Thiault, G.; Mellouki, A.; Le Bras, G.; Chakir, A.; Sokolowski-Gomez, N.; Daumont, D. *J. Photochem. Photobiol., A: Chem.* **2004**, *162*, 73−281.

(18) Etzkorn, T.; Klotz, B.; Sorensen, S.; Patroescu, I. V.; Barnes, I.; Becker, K. H.; Platt, U. *Atmos. Environ.* **1999**, *33*, 525.

(19) Fenter, F. F.; Nozière, B.; Caralp, F.; Lesclaux, R. *Int. J. Chem. Kinet*. **1994**, *26*, 171.

(20) Atkinson, R.; Baulch, D. L.; Cox, R. A.; Crowley, J. N.; Hampson, R. F.; Kerr, J. A.; Rossi, M. J.; Troe, J. *IUPAC Subcomm. Gas Kinet. Data Eval. Atmos. Chem. Web Ver.* **2003**, *Nov*, 1−58.

(21) Tsang, W. Chemical kinetic database for combustion chemistry. Part 2. Methanol. *J. Phys. Chem. Ref. Data* **1987**, *16*, 471.

(22) Pagsberg, P.; Munk, J.; Sillesen, A.; Anastasi, C. *Chem. Phys. Lett.* **1988**, *146*, 375.